First-principles study on the stability and photoelectric properties of lead-free double perovskites Cs_2TlSbI_6 and Rb_2TlSbI_6

YAN-LING TANG, GUANG-FU BAI[*], JIAN TANG, LIANG XU, GUANG-XIN WANG, DUN-SHENG SHANG
School of Physics, Guizhou University, Guiyang 550025, China

In this paper, the stability and photoelectric properties of lead-free double perovskites Cs_2TlSbI_6 and Rb_2TlSbI_6 were explored based on first-principles calculations. The thermodynamical, and mechanical stability of two perovskites are guaranteed by the negative formation enthalpy and Born-Huang stability criterion. The elastic constants show that two perovskites are ductile and anisotropic. The calculated band gap values are 1.196 eV for Cs_2TlSbI_6 and 1.103 eV for Rb_2TlSbI_6, respectively. Moreover, the perovskites Cs_2TlSbI_6 and Rb_2TlSbI_6 exhibit great light absorption, dielectric function, and conductivity. In conclusion, the perovskites Cs_2TlSbI_6 and Rb_2TlSbI_6 are suitable for solar cells due to their great photoelectric performances.

1. Introduction

With the gradual consuming of fossil energy, human beings need to explore an environmentally friendly energy source. As a clean energy, solar energy is renewable and can be converted to electrical energy through solar cells [1]. In the field of solar cells, perovskite solar cells (PSCs) exhibit considerable light absorption and high photoelectric conversion efficiency (PCE). In the past decade. The verified PCE of PSCs has reached 25.2% from the initial 3.8% [2], which enables the PSCs to be hopeful for high-quality solar cells. However, general organic-inorganic hybrid halide perovskites are generally toxic and unstable, which restricts these perovskites to be commercial extensively. For this background, it is particularly necessary to search for novel and stable materials as substitutes [3-5].

Fortunately, the double perovskites with the chemical formula $A_2BB'X_6$ have been proposed as effective alternatives for photoelectric devices due to their non-toxic and stable properties [6-13]. McClure et al reported that the perovskite $Cs_2AgBiBr_6$ and $Cs_2AgBiCl_6$ show great stability, and exhibit band gaps of 2.19 eV and 2.77 eV, respectively [6]. Moreover, the perovskite $Cs_2AgInCl_6$ has been synthesized in the experiment [7]. Zhang et al reported that the perovskite Cs_2NaBiI_6 exhibits a narrow direct band gap value (1.69 eV) and great stability [8]. The absorber layer based on the Cs_2TiBr_6 can improve the power conversion of an solar cell, and a power conversion of 16.85% is reported [9]. Cs_2TeI_6 [10], Cs_2PtI_6 [11], Cs_2PdBr_6 [12], and $Cs_2TiI_xBr_{6-x}$ [3] have been rated as potential perovskite solar cell candidates due to their suitable band gaps and environmental stability. Since the experimental synthesis of materials is time-consuming and

high-cost, many researchers seek new halide double perovskites theoretically based on first-principles calculations. Tariq et al. reported that the double perovskites Cs_2AgInX_6 (X=F, Cl, Br, I) are promising for photoelectric or thermoelectric devices based on their simulation work [13]. Varadwaj et al., Kibbou et al., and Saeed et al have systematically predicted the application potential of perovskites $Cs_2AgRhCl_6$ [14], Cs_2InGaX_6 (X=Cl, Br, or I) [15]. Cs_2InBiX_6 (X = F, Cl, Br, I) [16] in photoelectric devices.

Recently, Chen et al have reported that the perovskites Cs_2TlSbI_6 and Rb_2TlSbI_6 are considered candidates for solar cells [17]. However, they didn't discuss the stability and light absorption of these two perovskites, the relevant investigations are lacking so far. When studying the photoelectric features of perovskites, it's necessary to consider their stability at the same time. To further understand the properties of the perovskites Cs_2TlSbI_6 and Rb_2TlSbI_6, we conducted a simulation work to systematically explore their structural, electronic, optical, and elastic properties. The results show that the studied perovskites Cs_2TlSbI_6 and Rb_2TlSbI_6 are stable. Moreover, they exhibit superior light absorption in the visible light range. Therefore, they have great application potential in solar cells and other photoelectric devices. This work can provide a theoretical basis for the research and design of the perovskite Cs_2TlSbI_6 and Rb_2TlSbI_6, and promote their application in photoelectric devices.

2. Computational details

The calculations were performed by using the CASTEP module in Materials Studio software [18]. The

crystal structures were optimized using the BFGS minimizer [19]. The exchange-correlation term in the theoretical calculations was processed adopting the generalized gradient approximation of the Perdew–Burke–Ernzerhof (GGA-PBE) functional [20] because it was more effective in comparison to other GGA characteristics for geometry optimization [21]. Simultaneously, to process the electron-ion interactions, the plane-wave energy cutoff for ultra-soft pseudopotentials [22] was set as 550 eV. Additionally, the k-point grid was set to $10 \times 10 \times 10$ to sample the Brillouin zone. There were several convergence criteria including 5.0×10^{-4} Å for maximum displacement, 0.01 eV/Å for maximum force, 0.02 GPa for maximum stress and 5.0×10^{-6} eV/atom for energy. Moreover, the GGA-PBE was also utilized to study elastic properties, with convergence criteria including 1.0×10^{-4} Å for maximum displacement, 0.002 eV/Å for maximum force and 5.0×10^{-6} eV/atom for energy. Frequently, the band gaps of materials are underrated by the GGA-PBE functional because the exchange-correlation energy is discontinuous [23-24]. Several other functionals, such as the HSE06, can reach excellent consensus with the experimental results [25-26]. With a k-point grid of $3 \times 3 \times 3$ and an energy cutoff of 480 eV, the HSE06 functional was adopted to precisely investigate the electronic structures and optical properties of both compounds.

3. Results and discussion

3.1. Thermodynamic stability analysis

Thermodynamic stability is the foundation of material and is decided by the crystal structures. Accordingly, we first study the crystal structures of both compounds. Fig. 1 presents the fully optimized crystal structures of Cs_2TlSbI_6 and Rb_2TlSbI_6, which indicates that both compounds exhibit cubic phase structures. The crystal structures of Cs_2TlSbI_6 (Rb_2TlSbI_6) consist of an TlI_6 octahedron and SbI_6 octahedron, and the Cs_2TlSbI_6 (Rb_2TlSbI_6) appears octahedrons the alternant structure. The Cs (Rb) atom occupies the center of the octahedra. The Cs (Rb), Tl, Sb and I atoms occupy the 8c (0.25, 0.25, 0.25), 4a (0.50, 0.50, 0.50), 4b (0.00, 0.50, 0.50) and 24e (x, 0.00, 0.50) positions, respectively. The oxidation state on Cs (Rb) and Tl is +1, on Sb is +3 and on I is −1. The calculated results of crystal parameters of Cs_2TlSbI_6 and Rb_2TlSbI_6 are listed in Table 1. It can be found that the lattice constants of Cs_2TlSbI_6 and Rb_2TlSbI_6 are 12.720 and 12.620 Å. Besides, the values of x are 0.262 and 0.260 for Cs_2TlSbI_6 and Rb_2TlSbI_6, respectively.
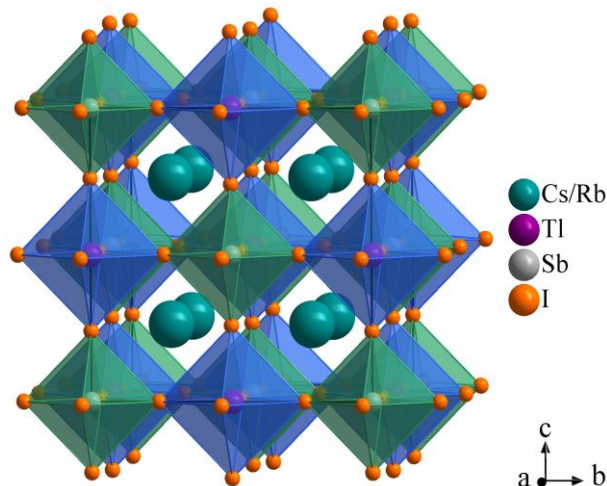

Fig. 1. The crystal structures of Cs_2TlSbI_6 and Rb_2TlSbI_6 (color online)

To analyze the thermodynamic stability of these two perovskites, the formation enthalpy ΔH [27] was calculated using the GGA-PBE method. The ΔH can be expressed as follows:

$$\Delta H = \frac{1}{10}\left(E_{Cs/Rb_2TlSbI_6} - 2E_{Cs/Rb} - E_{Tl} - E_{Sb} - 6E_I \right) \qquad (1)$$

where E_{Cs/Rb_2TlSbI_6} is the total energy of the perovskite material compounds and $E_{Cs/Rb}$, E_{Tl}, E_{Sb} and E_I are the energy of individual atoms, respectively. The values of ΔH are negative, therefore, the perovskites Cs_2TlSbI_6 and Rb_2TlSbI_6 are thermodynamically stable [27]. Moreover, the Cs_2TlSbI_6 has better stability than Rb_2TlSbI_6 due to its lower formation enthalpy.

Table 1. The predicted lattice constants a, value of x and formation enthalpy ΔH adopting the GGA-PBE functional

Parameters	Cs_2TlSbI_6	Rb_2TlSbI_6
a (Å)	12.720	12.620
x	0.262	0.260
ΔH (eV/atom)	−1.192	−1.130

3.2. Electronic properties

The electronic properties of a material, especially band structures, are essential to illustrate whether the material is suitable for solar cells. Hence, the electronic properties have been calculated by using the HSE06 functional after completing the structure optimization. The

predicted band gaps of Cs$_2$TlSbI$_6$ and Rb$_2$TlSbI$_6$ are 1.196 eV and 1.013 eV separately that conforms well to the results in the reference [17], indicating that both Cs$_2$TlSbI$_6$ and Rb$_2$TlSbI$_6$ have appropriate band gaps for solar cells. The predicted band structures of Cs$_2$TlSbI$_6$ and Rb$_2$TlSbI$_6$ are shown in Fig. 2. The band characteristics of the two materials near the CBM and VBM are similar to each other. It can be seen that the CBM and VBM locate at the same symmetry point (G), which indicates that both perovskite materials are direct bandgap semiconductors.
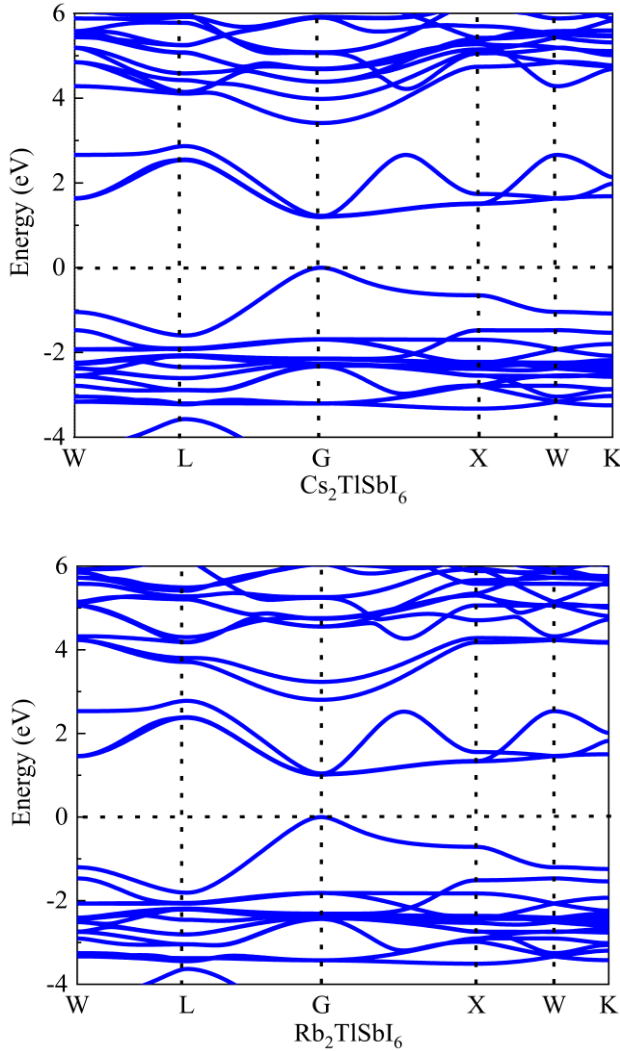

Fig. 2. The calculated band structures of Cs$_2$TlSbI$_6$ and Rb$_2$TlSbI$_6$

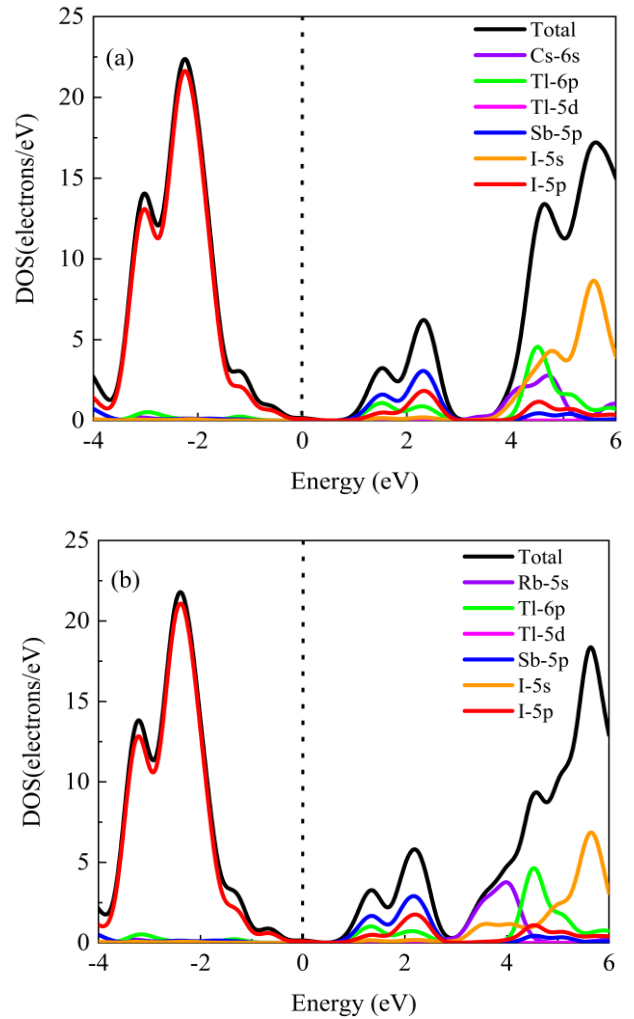*Fig. 3. The total and partial DOS of Cs$_2$TlSbI$_6$ (a) and Rb$_2$TlSbI$_6$ (b) (color online)*

The density of states (DOS) of both materials has been also forecasted based on HSE06 functional to further study the electronic properties. The total and partial DOS of both compounds are given in Fig. 3. The VBM is predominantly occupied by I-5p orbitals. The CBM is derived mainly from Sb-5p, Tl-6p, and I-5p orbitals, which demonstrates that there is a strong hybridization among Sb-5p orbitals along with Tl-6p and I-5p orbitals. As can be seen from Fig. 3, whether it is a Cs or Rb atom, it contributes to the energy area of around 3–5 eV.

The effective mass of charge carriers is related to the transport properties, such as carrier mobility. Therefore, we calculated the effective masse of electrons and holes for Cs$_2$TlSbI$_6$ and Rb$_2$TlSbI$_6$. The calculated results are listed in Table 2. It can be seen that both two compounds exhibit is relatively small.

Table 2. The calculated effective mass of electron (m_e)

and hole (m_h) *of two compounds*

	$m_e^*(m_0)$	$m_h^*(m_0)$
Cs_2TlSbI_6	0.16	0.19
Rb_2TlSbI_6	0.15	0.17

3.3. Optical properties

Besides electronic properties, the optical properties, especially optical absorption, are also important to decide whether a material is suitable for solar cell applications. Accordingly, the optical properties of both Cs_2TlSbI_6 and Rb_2TlSbI_6 have been calculated by using HSE06 functional. It is worth explaining that the complex dielectric function plays a fundamental role in all optical property parameters because other optical parameters such

as the absorption coefficient $\alpha(\omega)$, reflectivity $R(\omega)$, optical conductivity $\sigma(\omega)$, loss function $L(\omega)$, extinction coefficient $k(\omega)$ and refractive index $n(\omega)$ can be deduced from it. The complex dielectric function can be described as follows [28]:

$$\varepsilon(\omega) = \varepsilon_1(\omega) + i\varepsilon_2(\omega) \tag{2}$$

Here $\varepsilon_1(\omega)$ and $\varepsilon_2(\omega)$ work as the real and imaginary parts. Specifically, the $\varepsilon_1(\omega)$ describes the polarization of a material relying on the electric field from the external environment, whereas the $\varepsilon_2(\omega)$ is relevant to the optical absorption.
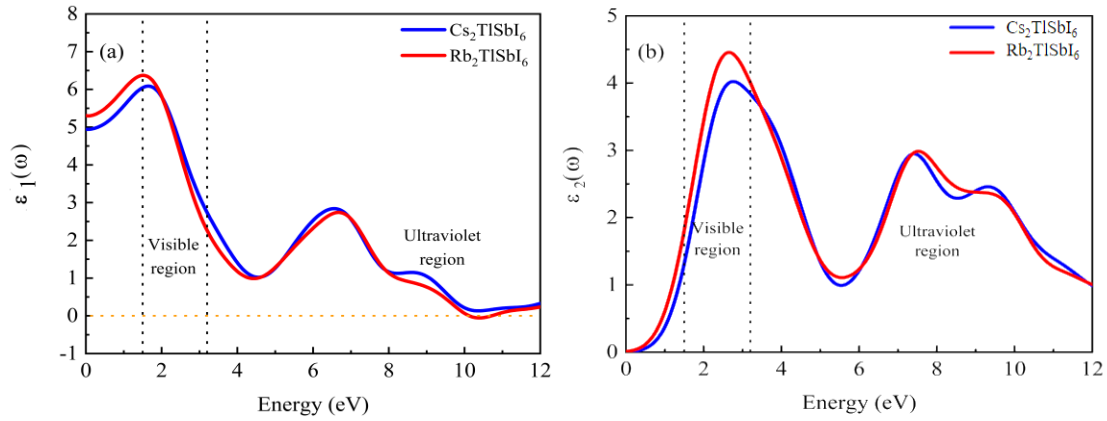

Fig. 4. The calculated real part $\varepsilon_1(\omega)$ *(a) and imaginary part* $\varepsilon_2(\omega)$ *(b) of dielectric functions of* Cs_2TlSbI_6

and Rb_2TlSbI_6 *(color online)*

The dielectric functions of Cs_2TlSbI_6 and Rb_2TlSbI_6 are displayed in Fig. 4. It can be seen that the real parts of both compounds are similar to each other, resulting from their similar electronic structures near the CBM and VBM. As can be seen from Fig. 4(a), $\varepsilon_1(\omega)$ have the highest values in the visible region. And after the maximum, $\varepsilon_1(\omega)$ gradually decrease and reach the sub-maximum value at around 6.60 eV in the the ultraviolet region. As a result, for each compound, the curve of $\varepsilon_1(\omega)$ forms two main peaks at around 1.63 and 6.60 eV, respectively, and one is in visible region and the other is in ultraviolet area.

It is worth explaining that the $\varepsilon_1(\omega)$ of Rb_2TlSbI_6 is below zero in the area of 10.13−10.72 eV, indicating the metallic behaviour [29]. The $\varepsilon_2(\omega)$ of both compounds show similarities to each other but a little difference, in which Cs_2TlSbI_6 has three dominant spectra peaks while Rb_2TlSbI_6 has two ones. The spectra peaks of Rb_2TlSbI_6 are particularly closed to the former two ones of Cs_2TlSbI_6, which locate at around 2.70 eV and 7.64 eV,

respectively, ranging from the visible region to ultraviolet ones. The other peak of Cs_2TlSbI_6 locates at 9.32 eV. It can be concluded that the highest peaks of these two compounds are at about 2.70 eV. Furthermore, we can obtain the conclusion that the first absorption peak of $\varepsilon_2(\omega)$ principally originates from the electronic transition from VBM to CBM via the comparison of DOS and band structures of these two compounds.

Several important optical parameters ie. $n(\omega)$, $k(\omega)$, $R(\omega)$ and $\alpha(\omega)$ are indispensable to entirely explore the optical properties of Cs_2TlSbI_6 and Rb_2TlSbI_6. These parameters can be directly or indirectly attained via the complex dielectric function as follows [30,31]:

$$n(\omega) = \left[\frac{\varepsilon_1(\omega)}{2} + \frac{\sqrt{\varepsilon_1^2(\omega) + \varepsilon_2^2(\omega)}}{2}\right]^{1/2} \tag{3}$$

$$k(\omega) = \left[-\frac{\varepsilon_1(\omega)}{2} + \frac{\sqrt{\varepsilon_1^2(\omega) + \varepsilon_2^2(\omega)}}{2}\right]^{1/2} \tag{4}$$

$$R(\omega) = \frac{\left[n(\omega)-1\right]^2 + k^2(\omega)}{\left[n(\omega)+1\right]^2 + k^2(\omega)} \quad (5)$$

$$\alpha(\omega) = \sqrt{2}\omega\left[\sqrt{\varepsilon_1^2(\omega)+\varepsilon_2^2(\omega)} - \varepsilon_1(\omega)\right]^{1/2} \quad (6)$$

The calculated optical parameters for Cs_2TlSbI_6 and Rb_2TlSbI_6 are presented in Fig. 5. The extinction coefficient $n(\omega)$ in Fig. 5(a) can measure the degree of attenuation of light during material propagation. In comparison to Fig. 4(a), it can be concluded that $n(\omega)$ exhibits similar trend as $\varepsilon_1(\omega)$, especially at which the peaks locate, demonstrating that the predicted results conform well to the relationships between these two optical parameters. The predicted values of $n(0)$ are 2.223 and 2.304 for Cs_2TlSbI_6 and Rb_2TlSbI_6, respectively, which are relevant to $\varepsilon_1(0)$ based on the relationship $n(0) = \sqrt{\varepsilon_1(0)}$ [32]. The curves of extinction coefficient $k(\omega)$ is presented in Fig. 5(b), which represents the degree of light absorption of the material when the light propagates within the material. It can be seen that the perovskite Rb_2TlSbI_6 exhibits higher $k(\omega)$ values within

the studied energy range. The curved lines of reflectivity $R(\omega)$ of Cs_2TlSbI_6 and Rb_2TlSbI_6 are presented in Fig. 5(c), which characterizes the degree of reflection on the surface of two compounds. The $R(0)$ is 0.144 for Cs_2TlSbI_6 and 0.156 for Rb_2TlSbI_6. Additionally, the maximum values of $R(\omega)$ of Cs_2TlSbI_6 and Rb_2TlSbI_6 are 0.207 at 2.409 eV and 0.220 at 2.396 eV, which pertain to the visible region. To get better comparison and observation, the $\varepsilon_1(0)$, $n(0)$, and $R(0)$ of both compounds are listed in Table 3. The absorption coefficient $\alpha(\omega)$ of Cs_2TlSbI_6 and Rb_2TlSbI_6 are utilized to describe the capability of solar energy storage, displayed in Fig. 5(d). As shown in the Fig. 5(d), there are three main absorption peaks in the ultraviolet range for Cs_2TlSbI_6 and simultaneously, with two chief absorption peaks, Rb_2TlSbI_6 also exhibits strong absorption in the ultraviolet area. Besides, both materials show good absorption in the visible range as well. Moreover, for the $\alpha(\omega)$ of Cs_2TlSbI_6 and Rb_2TlSbI_6, the higher the photon energy, the stronger the intensity of the peaks. In conclusion, the optical absorption of Cs_2TlSbI_6 and Rb_2TlSbI_6 in the visible and ultraviolet ranges proves their promising utilization for solar cell applications as well as other photovoltaic devices.
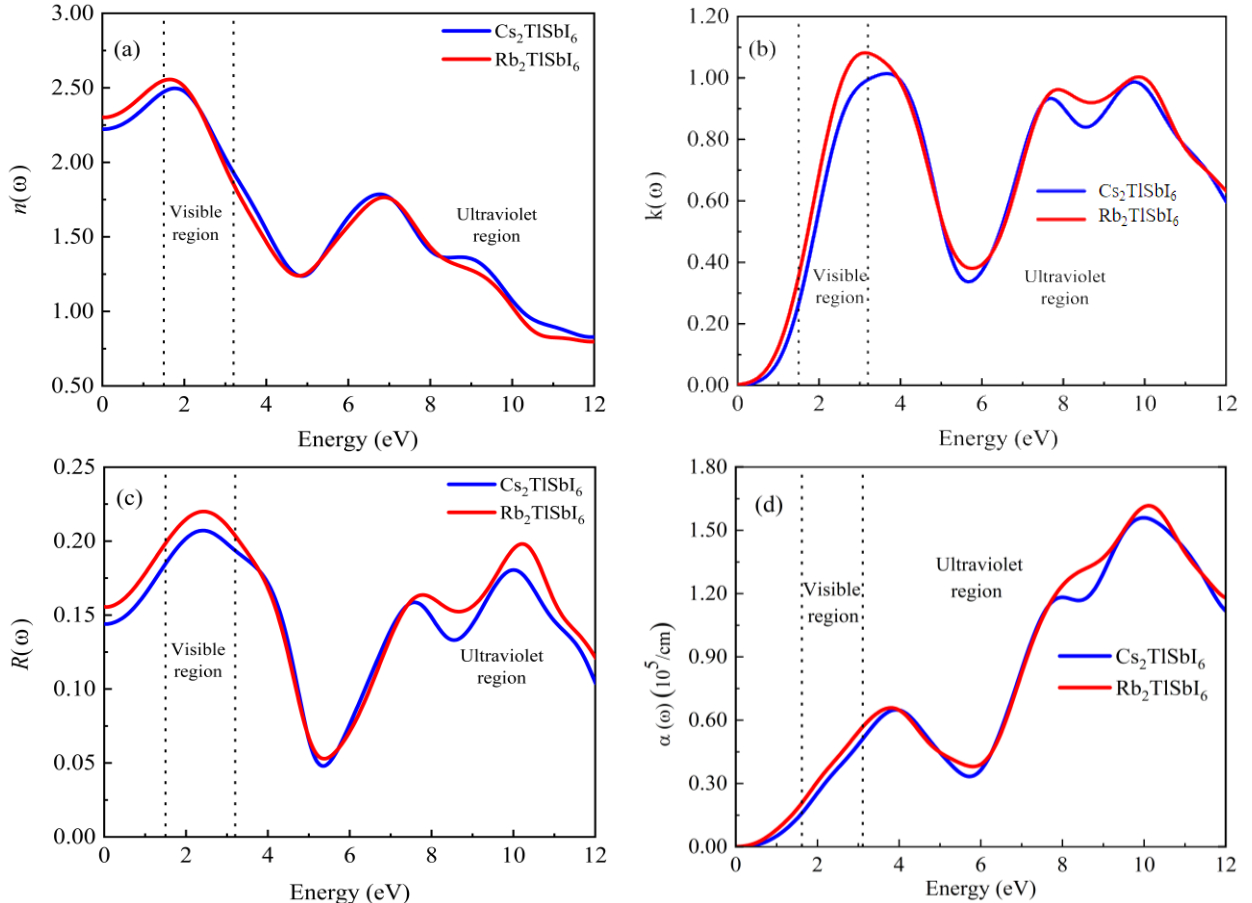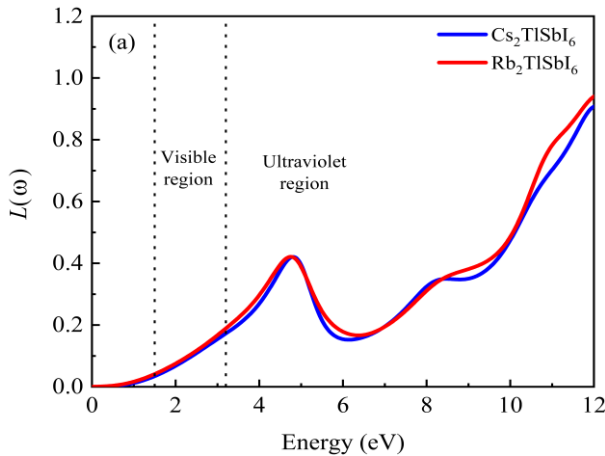

Fig. 5. The calculated $n(\omega)$, $k(\omega)$, $R(\omega)$ and $\alpha(\omega)$ of Cs_2TlSbI_6 and Rb_2TlSbI_6 (color online)

Table 3. The predicted results of $\varepsilon_1(0)$, $n(0)$ and $R(0)$ of Cs$_2$TlSbI$_6$ and Rb$_2$TlSbI$_6$

Compounds	$\varepsilon_1(0)$	$n(0)$	$R(0)$
Cs$_2$TlSbI$_6$	4.943	2.223	0.144
Rb$_2$TlSbI$_6$	5.306	2.304	0.156

The energy loss function $L(\omega)$, describing the energy decay of electrons passing through the materials, can be obtained using the following equation [31]:

$$L(\omega) = \text{Im}\left[\frac{-1}{\varepsilon(\omega)}\right] \tag{7}$$

The optical conductivity $\sigma(\omega)$ can be attained utilizing the relation [31] below:

$$\sigma(\omega) = i\frac{\omega}{4\pi}\left[\varepsilon(\omega) - 1\right] \tag{8}$$

The curved lines of energy loss function $L(\omega)$ of Cs$_2$TlSbI$_6$ and Rb$_2$TlSbI$_6$ are shown in Fig. 6(a). Before the curves reach their first peak, as the photon energy grows, the loss functions increase. After the curves pass through the first peak and then decrease to the minimal value at around 6.26 eV, the intensity of the loss function turns gradually high with the growing of energy. In fact, the loss functions of Cs$_2$TlSbI$_6$ and Rb$_2$TlSbI$_6$ are both tiny. The curves of the real part of the optical conductivity of Cs$_2$TlSbI$_6$ and Rb$_2$TlSbI$_6$ are shown in Fig. 6(b). It is obvious that the tendencies of the optical conductivity of both compounds are similar to each other. The curves show three chief peaks. The maximum values of optical conductivity are 2.793 at 9.476 eV for Cs$_2$TlSbI$_6$ and 2.741 at 7.656 eV for Rb$_2$TlSbI$_6$.
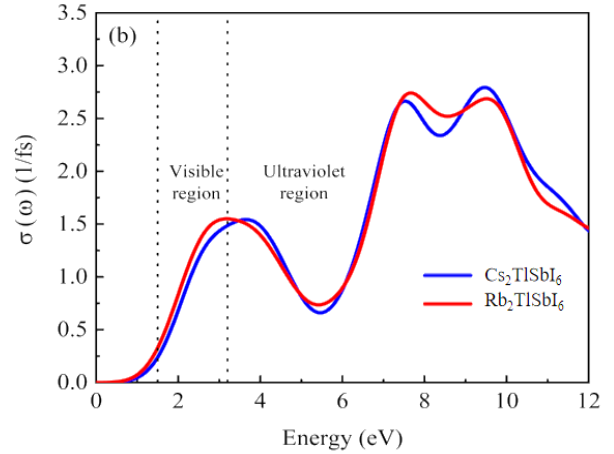

Fig. 6. The curves of $L(\omega)$ and $\sigma(\omega)$ for Cs$_2$TlSbI$_6$ and Rb$_2$TlSbI$_6$ (color online)

3.4. Elastic properties

To understand the mechanical stability and strength of the exterior force of both two materials, the elastic properties of Cs$_2$TlSbI$_6$ and Rb$_2$TlSbI$_6$ have been investigated. The calculated results are listed in Table 4.

Elastic constants play a fundamental role in all elastic properties and the calculated results of these parameters of Cs$_2$TlSbI$_6$ and Rb$_2$TlSbI$_6$ meet the Born mechanical stability criteria, which can be portrayed as $C_{11} + 2C_{12} > 0$, $C_{44} > 0$, and $C_{12} < C_{11}$ [33]. This indicates that both Cs$_2$TlSbI$_6$ and Rb$_2$TlSbI$_6$ are mechanically stable. The shear modulus (G), reflecting the ability that a material resists the reversible deformation under shear stress, can provide information about the stiffness of a solid material. G is predicted based on dual common models according to Voigt (G_V) [34] and Reuss (G_R) [34]:

$$G_V = \frac{1}{5}\left(3C_{44} + C_{11} - C_{12}\right) \tag{9}$$

$$G_R = \frac{5\left(C_{11} - C_{12}\right)C_{44}}{4C_{44} + 3\left(C_{11} - C_{12}\right)} \tag{10}$$

Moreover, there is another model according to Hill (G_H) for shear modulus, whose result is the arithmetic mean of G_V and G_R,

$$G_H = \frac{G_V + G_R}{2} \tag{11}$$

From the results, it can be concluded that the shear modulus of Cs$_2$TlSbI$_6$ has a higher value of 5.960 *GPa*, clarifying that it is more rigid than Rb$_2$TlSbI$_6$.

Young's modulus (Y) determines the response of a material to linear deformation such as the obdurability relying on Y [16]. The obdurability of a material will be greater when Y is larger. The higher Y (15.495) for Cs_2TlSbI_6 states clearly that it is tougher than Rb_2TlSbI_6. The ductility or brittleness of material is necessary for practical applications. Frequently, Pugh's ratio (B/G) is useful to describe the ductility or brittleness of a material [32]. Provided B/G is below 1.75, the material is of brittleness, otherwise it is of ductility. In addition, the Poisson ratio which can be adopted to differentiate ductile materials from brittle ones as well, was calculated according to the following formula:

$$\nu = \frac{3B-Y}{6B} \qquad (12)$$

Based on the reference [35], the Poisson ratio is below 0.26 for brittle materials and above 0.26 for ductile ones. Poisson and Pugh's ratios results both demonstrate that these two perovskites are ductile materials. The other important parameter to fully understand the elastic properties is the anisotropic parameter A, whose expression can be given as

$$A = \frac{2C_{44}}{C_{11}-C_{12}} \qquad (13)$$

An ideal isotropic system is characterized by that the value of A is unity. However, for the anisotropic material, A differs from unity. It can be found that both compounds are anisotropic because their values of A diverge from unity.

Table 4. The predicted results of C_{ij}, G, Y, B, B/G, ν and A.

Parameters	Cs_2TlSbI_6	Rb_2TlSbI_6
C_{11} (Gpa)	29.841	26.282
C_{12} (Gpa)	4.451	2.151
C_{44} (Gpa)	3.396	3.350
G_H (GPa)	5.960	5.774
Y (GPa)	15.495	14.571
B (GPa)	12.914	10.195
B/G (B/G_H)	2.167	1.766
ν	0.300	0.262
A	0.268	0.278

4. Conclusions

The stability and photoelectric properties of halide double perovskites Cs_2TlSbI_6 and Rb_2TlSbI_6 have been investigated via first-principles theoretical calculations in this study. The GGA-PBE functional has been utilized to study the thermodynamic and mechanical stability. The calculated results of negative formation enthalpy, -1.192 eV for Cs_2TlSbI_6 and -1.130 eV for Rb_2TlSbI_6, indicate that both materials are thermodynamic stable. The elastic constants calculated in this paper meet Born mechanical stability criteria, which ensures the mechanical stability of both compounds. The photoelectric properties of these two perovskites have been studied utilizing the HSE06 functional. For electronic properties, the calculated band structures demonstrate that both perovskites are direct bandgap semiconductors. The band gap values, 1.196 eV for Cs_2TlSbI_6 and 1.013 eV for Rb_2TlSbI_6, clarify that both perovskites are appropriate for solar cell applications. To reveal specific optical properties, several important optical parameters including optical absorption, loss function and so on have been investigated. The results demonstrate that Cs_2TlSbI_6 and Rb_2TlSbI_6 exhibit low optical loss and strong optical absorption. Due to their high stability and good photoelectric properties, especially narrow band gaps and strong optical absorption, both Cs_2TlSbI_6 and Rb_2TlSbI_6 are suitable for solar cell applications and other photoelectric devices.

References

[1] D. M. Chapin, C. S. Fuller, G. L. Pearson, J. Appl. Phys. **25**, 676 (1954).

[2] J. J. Yoo, G. Seo, M. R. Chua, T. G. Park, Y. Lu, F. Rotermund, Y. K. Kim, C. S. Moon, N. J. Jeon, J. P. C. Baena, V. Bulovic, S. S. Shin, M. G. Bawendi, J. Seo, Nature **590**, 587 (2021).

[3] M. G. Ju, M. Chen, Y. Y. Zhou, H. F. Garces, J. Dai, L. Ma, N. P. Padture, X. C. Zeng, ACS Energy Lett. **3**, 297 (2018).

[4] D. B. Straus, S. Guo, A. M. M. Abeykoon, R. J. Cava, Adv. Mater. **3**, 2001069 (2020).

[5] B. Conings, J. Drijkoningen, N. Gauquelin, A. Babayigit, J. D'Haen, L. D'Olieslaeger, A. Ethirajan, J. Verbeeck, J. Manca, E. Mosconi, F. De. Angelis, H. G. Boyen, Adv. Energy Mater. **5**, 1500477 (2015).

[6] E. T. McClure, M. R. Ball, W. Windl, P. M. Woodward, Chem Mater. **28**, 1348 (2016).

[7] G. Volonakis, A. A. Haghighirad, R. L. Milot, W. H. Sio, M. R. Filip, B. Wenger, M. B. Johnston, L. M. Herz, H. J. Snaith, F. Giustino, J. Phys. Chem. Lett. **8**, 772 (2017).

[8] C. Zhang, L. G. Gao, S. Teo, Z. L. Guo, Z. H. Xu, S.

Zhao, T. L. Ma, Sustain. Energ. Fuels **2**, 2419 (2018).

[9] S. A. Moiz, A. N. M. Alahmadi, Polymers **13**, 13 (2021).

[10] A. E. Maughan, A. M. Ganose, M. M. Bordelon, E. M. Miller, D. O. Scanlon, J. R. Neilson, J. Am. Chem. Soc. **138**, 8453 (2016).

[11] S. Z. Yang, L. Wang, S. Zhao, A. M. Liu, Y. Zhou, Q. J. Han, F. Y. Yu, L. G. Gao, T. L. Ma, ACS Appl. Mater. Inter. **12**, 44700 (2020).

[12] W. Ye, Q. Cao, X. F. Cheng, C. Yu, J. H. He, J. M. Lu, J. Mater. Chem. A **8**, 17675 (2020).

[13] M. Tariq, M. A. Ali, A. Laref, G. Murtaza, Solid State Commun. **314**, 113929 (2020).

[14] P. R. Varadwaj, H. M. Marques, Front Chem. **8**, 796 (2020).

[15] M. Kibbou, Z. Haman, I. Bouziani, N. Khossossi, Y. Benhouria, I. Essaoudi, A. Ainane, R. Ahujia, Curr. Appl. Phys. **21**, 50 (2021).

[16] M. Saeed, I. U. Haq, S. U. Rehman, A. Ali, W. A. Shah, Z. Ali, Q. Khan, I. Khan, Chin. Opt. Lett. **19**, 030004 (2021).

[17] X. W. Chen, C. Wang, Z. Z. Li, Z. F. Hou, W. J. Yin, Sci. China Mater. **63**, 1024 (2020).

[18] S. J. Clark, M. D. Segall, C. J. Pickard, P. J. Hasnip, M. I. J. Probert, K. Refson, M. C. Payne, Z Kristallogr. **220**, 567 (2005).

[19] B. G. Pfrommer, M. Cote, S. G. Louie, M. L. Cohen, J. Comput. Phys. **131**, 233 (1997).

[20] D. N. Trong, N. C. Cuong, D. Q. Van, J. Multi. Model. **11**(2), 2030001 (2020).

[21] H. Jiang, J. Chem. Phys. **134**, 204705 (2011).

[22] D. Vanderbilt, Phys. Rev. B **41**, 7892 (1990).

[23] J. Nisar, C. Arhammar, C. Jamstorp, R. Ahujia, Phys. Rev. B Cond. Matter. **84**, 2250 (2011).

[24] M. G. Jin, Z. B. Li, F. Huang, W. L. Wang, Mod. Phys. Lett. B **33**, 1950266 (2019).

[25] J. Feng, B. Xiao, J. Phys. Chem. Lett. **5**, 1719 (2014).

[26] J. Heyd, G. E. Scuseria, M. Ernzerhof, J. Chem. Phys. **124**, 8207 (2006).

[27] X. H. Zhao, X. N. Wei, T. Y. Tang, L. K. Gao, Q. Xie, L. M. Lu, Y. L. Tang, Opt. Mater. **114**, 110952 (2021).

[28] M. Fried, T. Lohner, W. Aarnink, J. Appl. Phys. **71**(10), 5260 (1992).

[29] A. Nyayban, S. Panda, A. Chowdhury, B. I. Sharma, Mater. Today Commun. **24**, 101190 (2020).

[30] M. Houari, B. Bouadjemi, A. Abbad, T. Lantri, S. Haid, W. Benstaali, M. Matougui, S. Bentata, JETP Lett. **112**, 364 (2020).

[31] Q. Mahmood, M. Yaseen, M. Hassan, S. M. Ramay, A. Mahmood, Chin. Phys. B **26**, 1 (2017).

[32] Q. Mahmood, T. Ghrib, A. Rached, A. Laref, M. A. Kamran, Mater. Sci. Semicond. Process. **112**, 105009 (2020).

[33] F. Mouhat, F. X. Coudert, Phys. Rev. B **90**, 224104 (2014).

[34] X. H. Zhao, F. Wang, D. Y. Hu, L. M. Lu, L. Li, T. Y. Tang, Y. L. Tang, J. Mol. Model. **2810**, 1 (2022).

[35] J. Feng, Apl. Mater. **2**, 081081 (2014).

*Corresponding author: baiguangfu123@163.com